EINAR H. GUÐMUNDSSON:

ÞYNGDARLINSUR

FUNDUR SÍ

24. SEPT. 1997

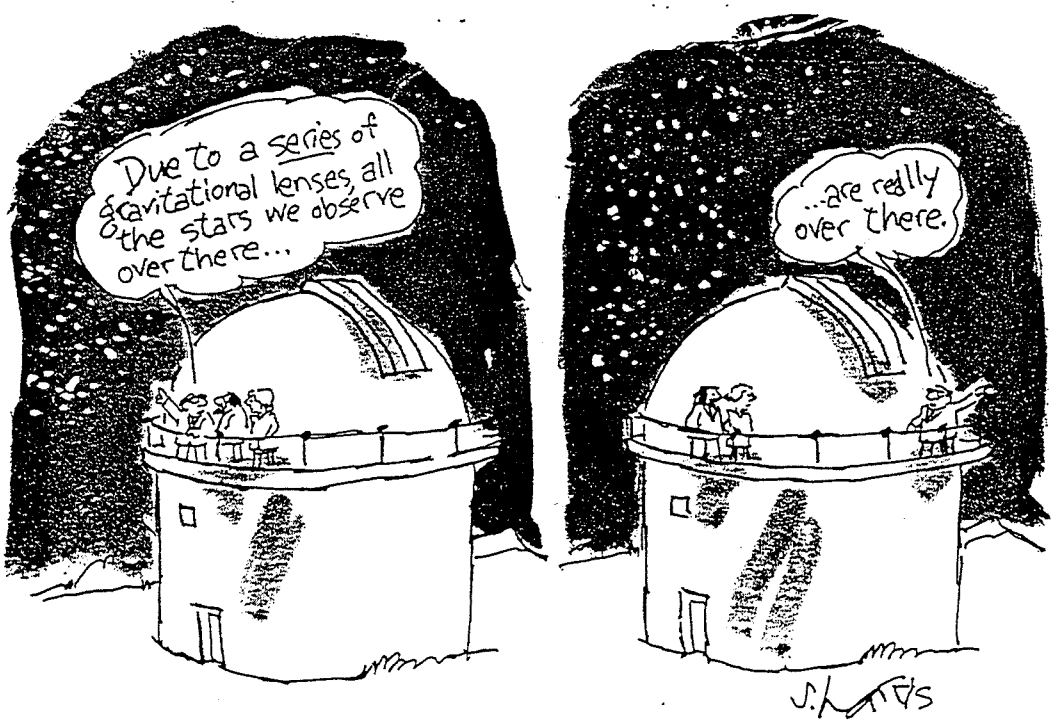

Stjarnvísindafélag Íslands

The Icelandic Astronomical Society

Dunhaga 3, IS-107 Reykjavík, Iceland

Telephone: +354 - 525 4800

Telefax: +354 - 552 8911

19. september 1997

Almennur félagsfundur verður haldinn í fundarherbergi Norræna hússins, miðvikudaginn 24. september 1997, kl. 16:00. Einar H. Guðmundsson mun þar segja frá þyngdarlinsum, en að því loknu verður rætt um afnot Íslendinga af Norræna sjónaukanum.

Félagsmenn eru hvattir til að mæta.

Stjórn S.Í.

SVEIGJA LJÓSS Í VEIKU ÞYNGDARSVIÐI

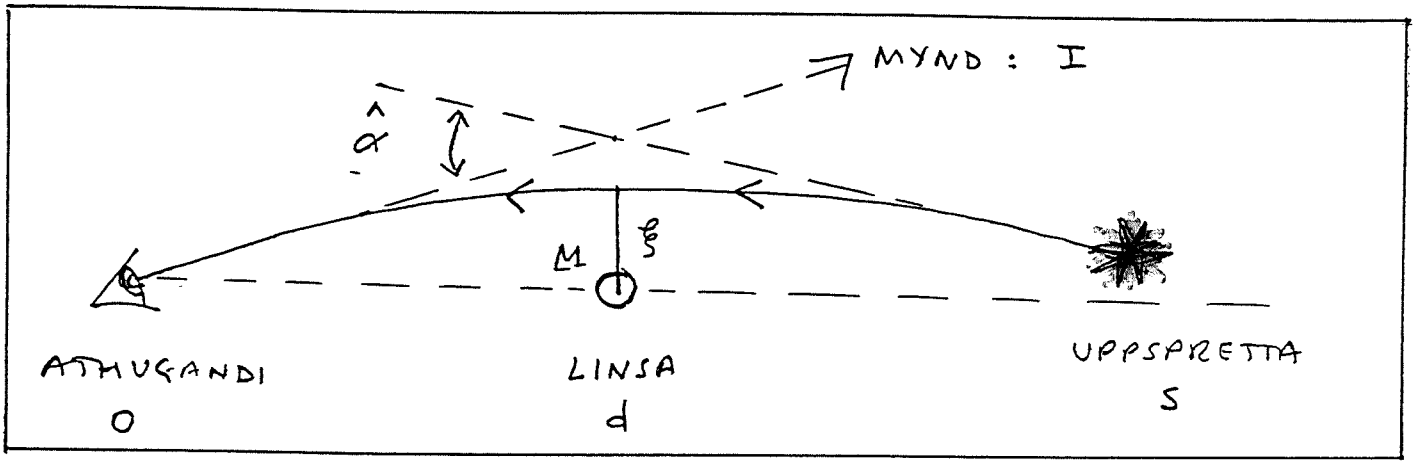

ALM. AFSTÆÐISK. :

$$\hat{\alpha} = \frac{4GM}{c^2 \xi} = \frac{2R_s}{\xi} \sim 1{,}75''$$

FYRIR RÖND SÓLAR

YFIRBORÐSBIRTA (SURFACE BRIGHTNESS) ER VARÐVEITT

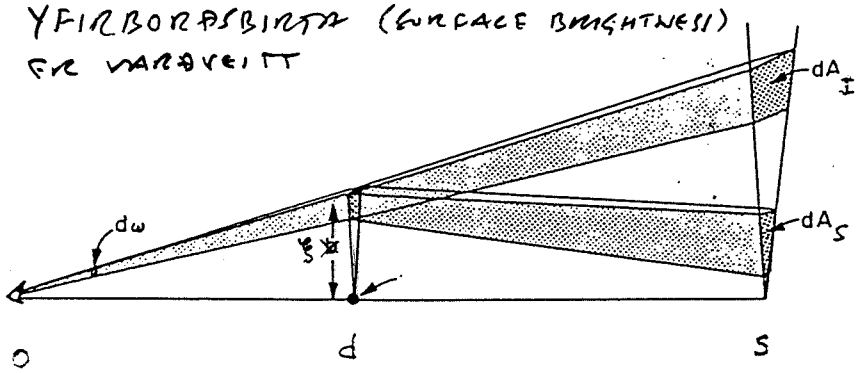

MÓÐGNUN / STÆKKUN : $\mu_I = \frac{dA_I}{dA_S}$

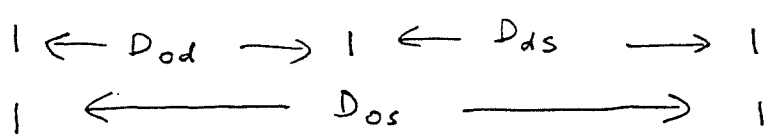

D-IN ERU SÝNDARFJARLÆGÐIR.

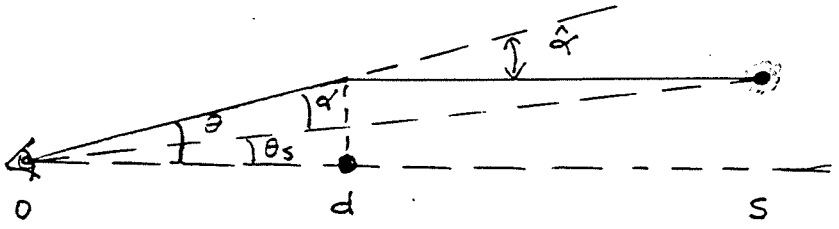

LÍTIL HORN :

$$\alpha = \frac{D_{ds}}{D_{os}} \hat{\alpha}$$

LINSUJAFNAN :

$$\alpha = \theta - \theta_s$$

GILDIR FYRIR SÉRHVERJA MYND !

PUNKTLINSA

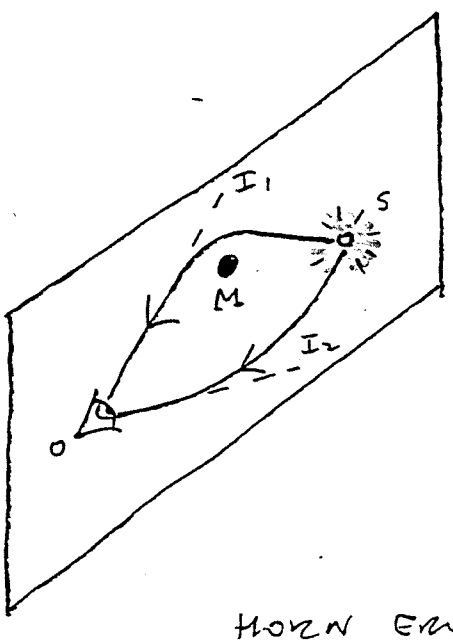

O
d
S
I_1
I_2

Í SAMA PLANI

$$\alpha_i = \theta_i - \theta_S \qquad i = 1,2$$

HÉR ER REIKNUÐ MEÐ FORMERKJUM

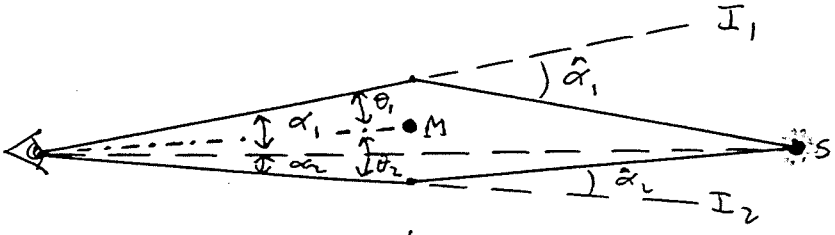

$$\Delta\theta = \theta_1 - \theta_2$$

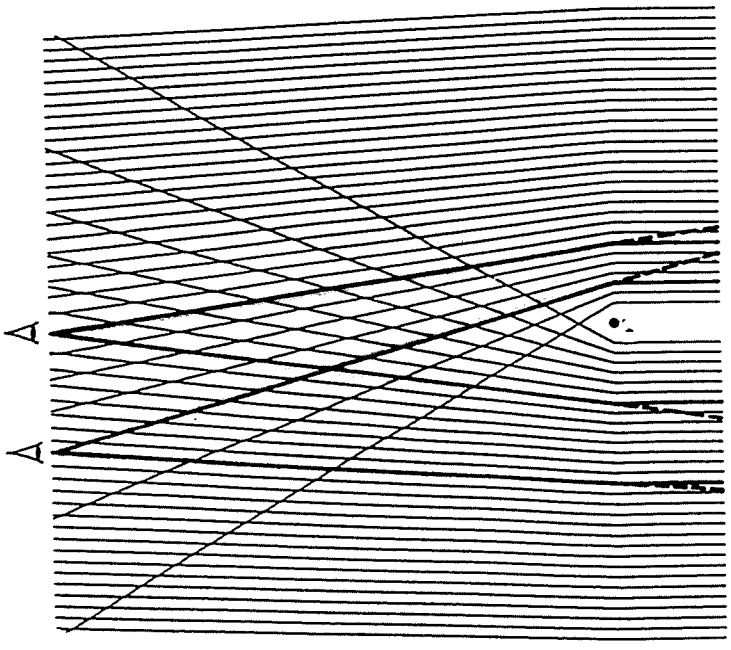

REFSDAL & SURDEJ
1994

PUNKTLINSA – FRAMHALD

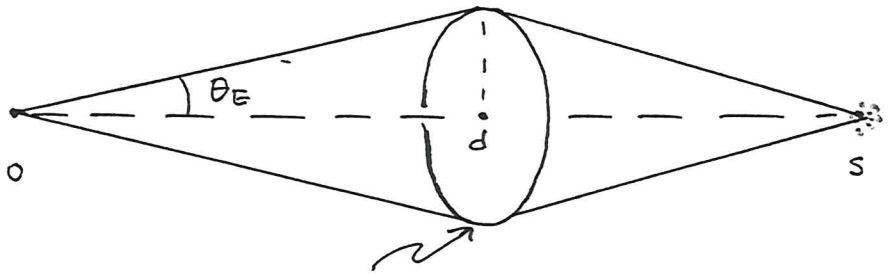

$$\theta_E = \left[\frac{2R_S}{\left(\frac{D_{Od} D_{OS}}{D_{dS}} \right)} \right]^{1/2}$$

EINSTEINSHRINGUR : O, d OG S LIGGJA Á BEINNI LÍNU

$$D \equiv \frac{D_{Od} D_{OS}}{D_{dS}} \rightarrow \theta_E = \left(\frac{2R_S}{D} \right)^{1/2} = 2{,}85 \; \mu\text{arcsec} \left(\frac{M/M_\odot}{D/\text{Gpc}} \right)^{1/2}$$

$$\theta_E \approx \begin{cases} 0{,}9 \text{ marcsec} \left(\frac{M}{M_\odot} \right)^{1/2} \left(\frac{D}{10\,\text{kpc}} \right)^{-1/2} \\ 2{,}85'' \left(\frac{M}{10^{12} M_\odot} \right)^{1/2} \left(\frac{D}{\text{Gpc}} \right)^{-1/2} \end{cases}$$

$$\theta = \theta_s \pm \sqrt{\theta_E^2 + \left(\frac{\theta_s}{2}\right)^2}$$

HORNFJARLÆGÐ I$_1$ OG I$_2$: $\Delta\theta = 2\sqrt{\theta_E^2 + \left(\frac{\theta_s}{2}\right)^2}$

EF $u \equiv \frac{\theta_s}{\theta_E}$ þá er :

$$\Delta\theta = \theta_E \sqrt{u^2+4}$$

$$\mu_1 = -\left[\frac{u^2+2}{2u(u^2+4)^{1/2}} - \frac{1}{2} \right]$$

(mynd víxlsnýst)

μ_1 OG μ_2 EKKI MÆLANL. S SÉST EKKI !

$$\mu_2 = \left[\frac{u^2+2}{2u(u^2+4)^{1/2}} + \frac{1}{2} \right] > 1$$

$$\mu = |\mu_1| + |\mu_2| = \frac{u^2+2}{u(u^2+4)^{1/2}} > 1$$

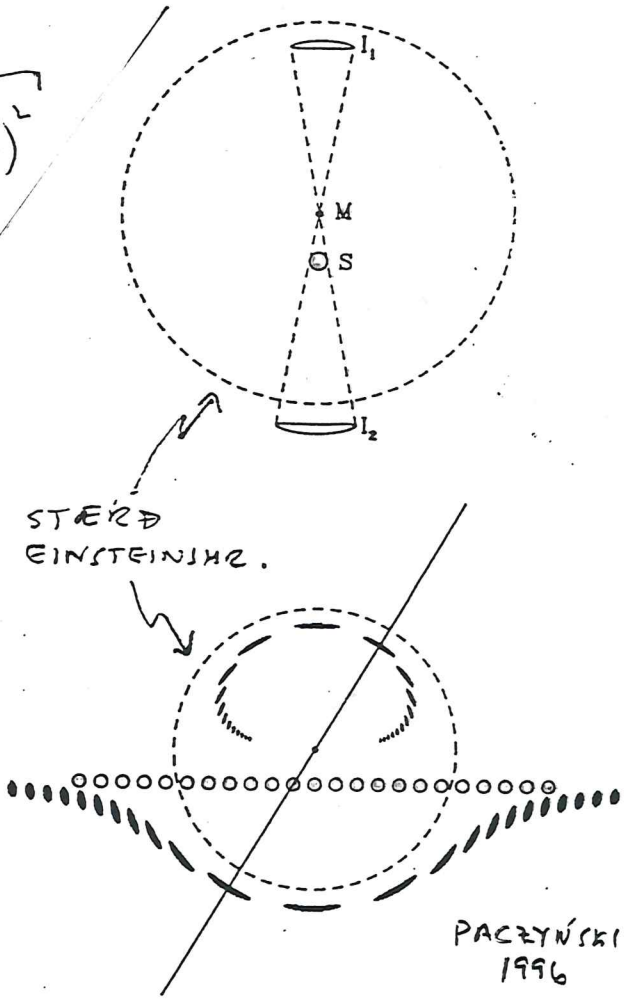

FLÓKNAR LINSUR

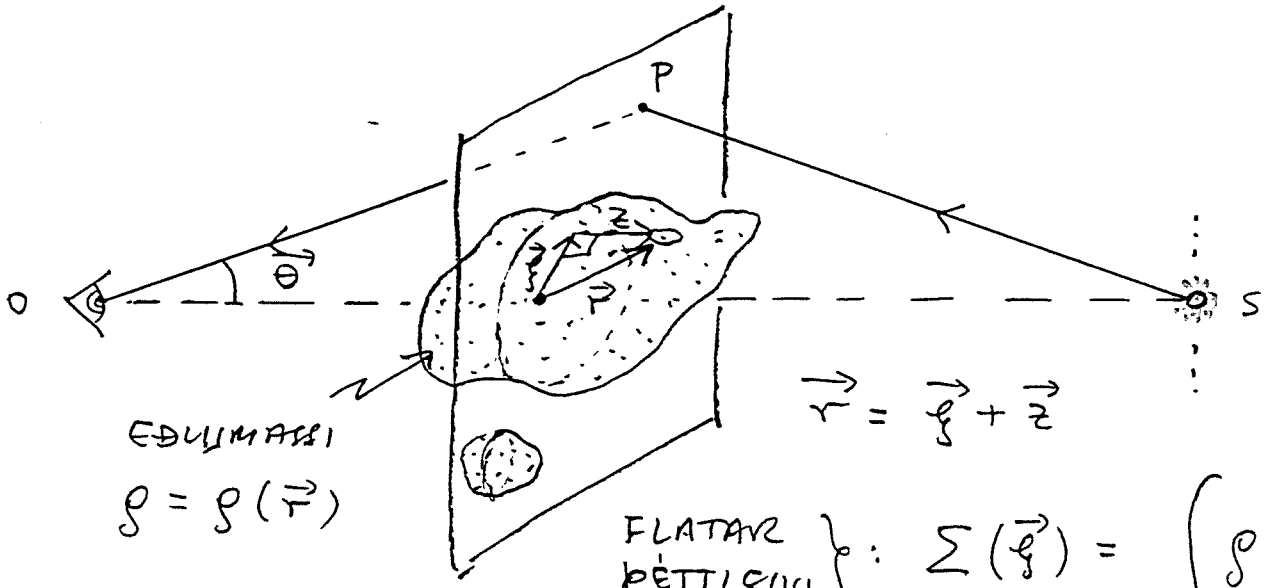

FLATAR ÞÉTTLEIKI: $\Sigma(\vec{\xi}) = \int_{\text{linsa}} \rho(\vec{\xi}, z)\, dz$

GAGNLEG VÍÐÁRSÆRISFERÐ: $\Sigma_{cr} = \frac{M}{\pi R_E^2} = \frac{c^2}{4\pi G}\frac{D_{os}}{D_{od} D_{ds}} \approx \frac{0{,}35\ g/cm^2}{(D'/Gpc)}$

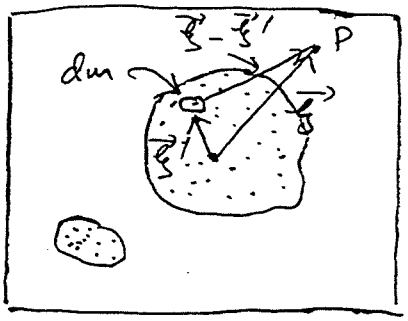

$dm = \Sigma(\vec{\xi}')\, d^2\xi'$

$d\hat{\alpha} = \frac{4G}{c^2}\frac{dm\,(\vec{\xi}-\vec{\xi}')}{|\vec{\xi}-\vec{\xi}'|^2}$

$d\vec{\alpha} = \frac{D_{ds}}{D_{os}}\, d\hat{\alpha}$

(EF $\Sigma < \Sigma_{cr}$ ÞÁ VERÐA ÞINSUMMUR VEIK)

$$\vec{\alpha} = \iint_{\text{linsa}} d\vec{\alpha} = \frac{D_{ds}4G}{D_{os}c^2}\iint_{\text{linsa}} \frac{(\vec{\xi}-\vec{\xi}')\,\Sigma(\vec{\xi}')\,d^2\xi'}{|\vec{\xi}-\vec{\xi}'|^2} = \frac{1}{\pi}\iint_{\text{linsa}} \kappa(\vec{\theta}')\frac{(\vec{\theta}-\vec{\theta}')}{|\vec{\theta}-\vec{\theta}'|^2}\, d^2\theta'$$

$$= \vec{\nabla}\psi$$

SAMLEITNI (CONVERGENCE)

ÞAR SEM $\kappa(\vec{\theta}) = \frac{\Sigma(\vec{\theta})}{\Sigma_{cr}}$, $\vec{\theta} = \frac{1}{D_{od}}\vec{\xi}$

OG ψ ER ÞRÍVÍÐA MÆTTI:

$$\psi(\vec{\theta}) = \left(\frac{D_{ds}}{D_{od}D_{os}}\right)\frac{2}{c^2}\int \Phi_{\text{Þrívíða NEWTÓNSKA ÞYNGDARMÆTTIÐ}}(\vec{\xi}, z)\, dz = \frac{1}{\pi}\iint_{\text{linsa}} \kappa(\vec{\theta}')\ln|\vec{\theta}-\vec{\theta}'|\, d^2\theta'$$

FLÓKNAR LINSUR – FRAMHALD

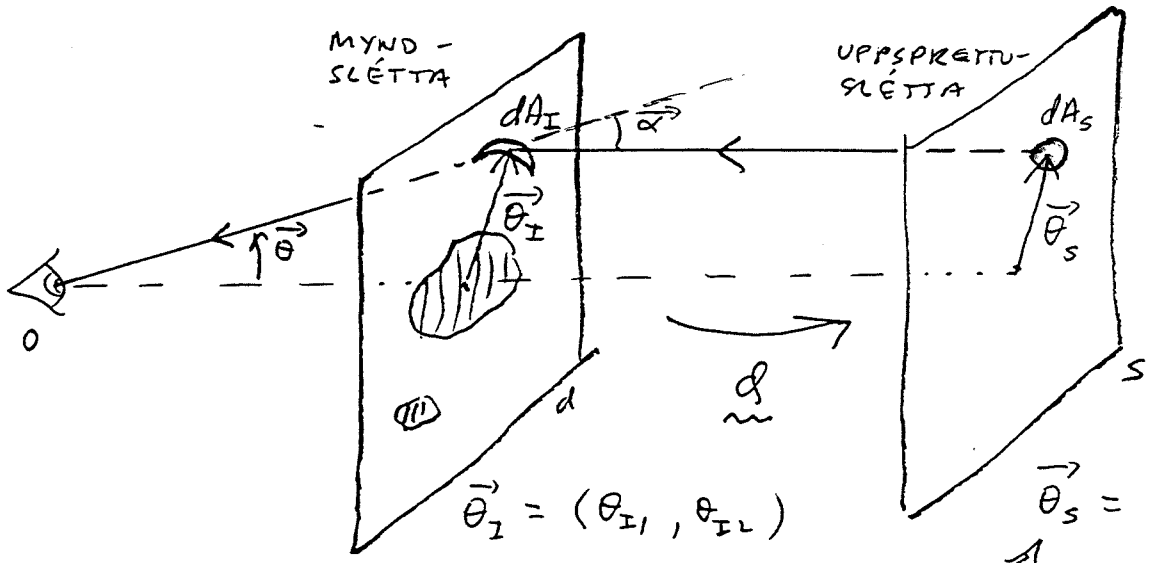

$$\left.\begin{aligned} \vec{\theta}_S &= \vec{\theta}_I - \vec{\alpha} \\ \left(\vec{\alpha} &= \frac{D_{ds}}{D_{os}}\hat{\alpha}\right) \\ \vec{\alpha} &= \vec{\nabla}\psi \end{aligned}\right\} : \quad \vec{\theta}_S = \vec{\theta}_I - \vec{\nabla}\psi$$

$\psi = \psi(\vec{\theta}_I)$

$\underset{\sim}{\varphi} : \vec{\theta}_I \to \vec{\theta}_S \quad \Rightarrow \quad dA_S = \det J \, dA_I$ þar sem J er

JAKOBI FYLKIÐ : $J = \begin{pmatrix} \frac{\partial\theta_{S1}}{\partial\theta_{I1}} & \frac{\partial\theta_{S2}}{\partial\theta_{I1}} \\ \frac{\partial\theta_{S1}}{\partial\theta_{I2}} & \frac{\partial\theta_{S2}}{\partial\theta_{I2}} \end{pmatrix} = \begin{pmatrix} 1-\frac{\partial^2\psi}{\partial\theta_{I1}^2} & -\frac{\partial^2\psi}{\partial\theta_{I1}\partial\theta_{I2}} \\ -\frac{\partial^2\psi}{\partial\theta_{I2}\partial\theta_{I1}} & 1-\frac{\partial^2\psi}{\partial\theta_{I2}^2} \end{pmatrix}$

ANDHVERFAN : $M = J^{-1}$ ER KALLAÐ MÖGNUNARFYLKIÐ þar sem

$$\mu = \frac{dA_I}{dA_S} = (\det J)^{-1} = \det M$$

EF $\det J = 0$ þÁ ER $\mu = \infty$:

{ S Á BRENNILÍNU (CAUSTIC)
I Á MARKLÍNU (CRITICAL CURVE)

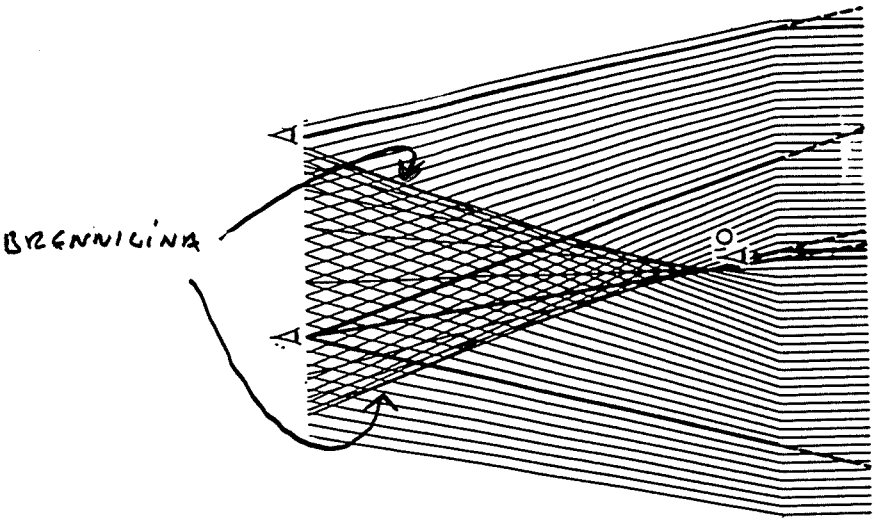

LINSA:
EINFALT LÍKAN
AF DYRÐLÞOKU

REFSDAL & SURDEJ 1994

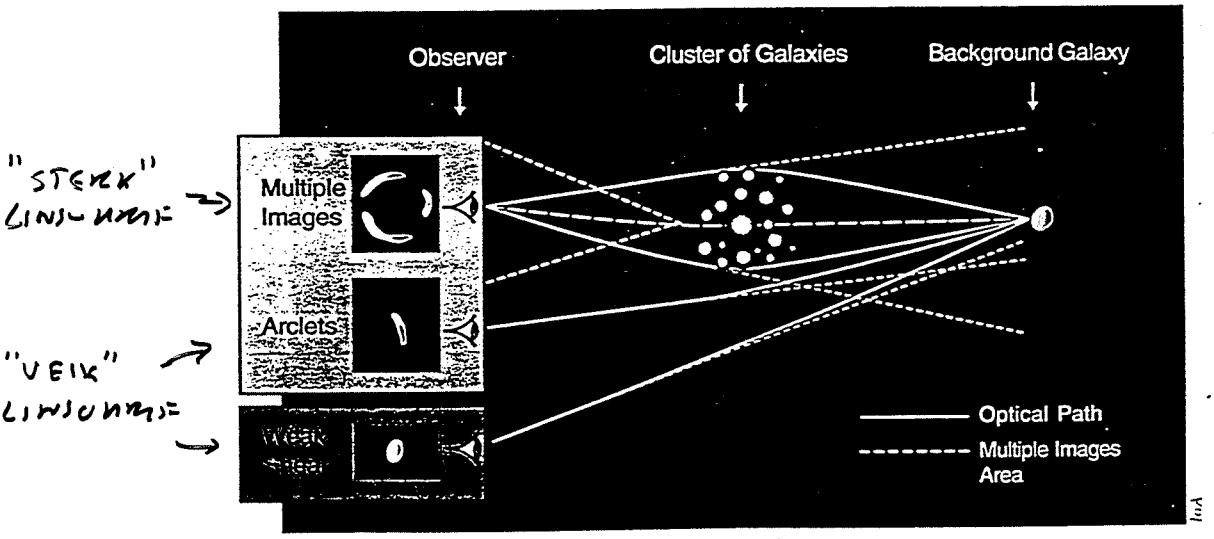

IOA CAMBRIDGE

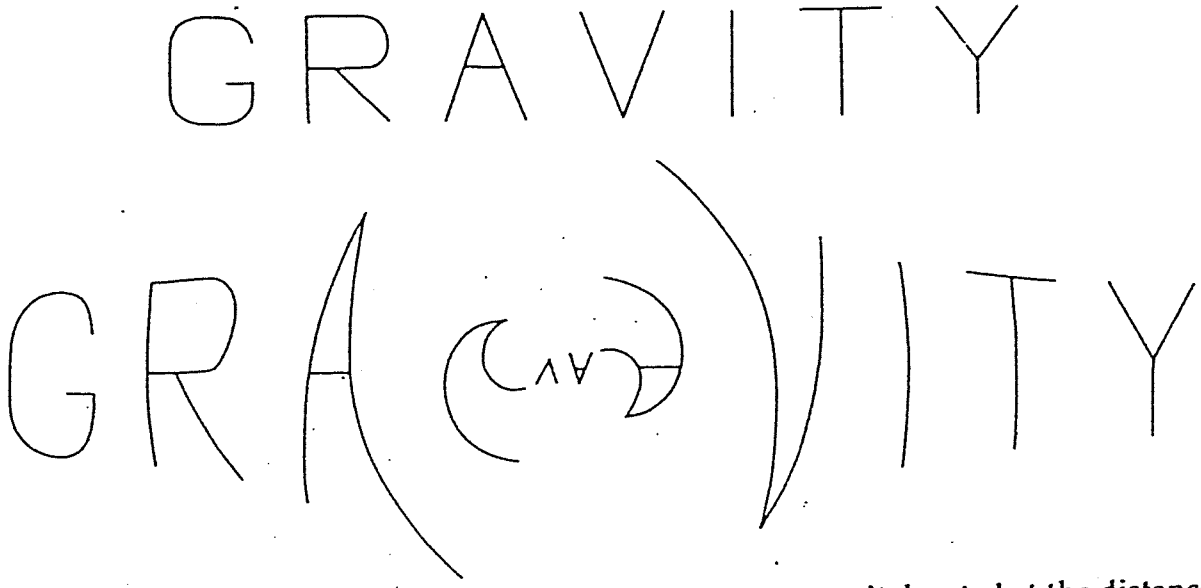

Figure 3. Imagine a giant billboard with the word GRAVITY on it, located at the distance of a typical quasar. If a spherical galaxy with a smooth mass distribution were placed halfway between us and the billboard, centered between the A and the V, and if its size were such that the critical bending angle included these two letters only, we would see only one image of GR and ITY, but three images each of A and V, two inverted, the other upright.

GOTT 1983

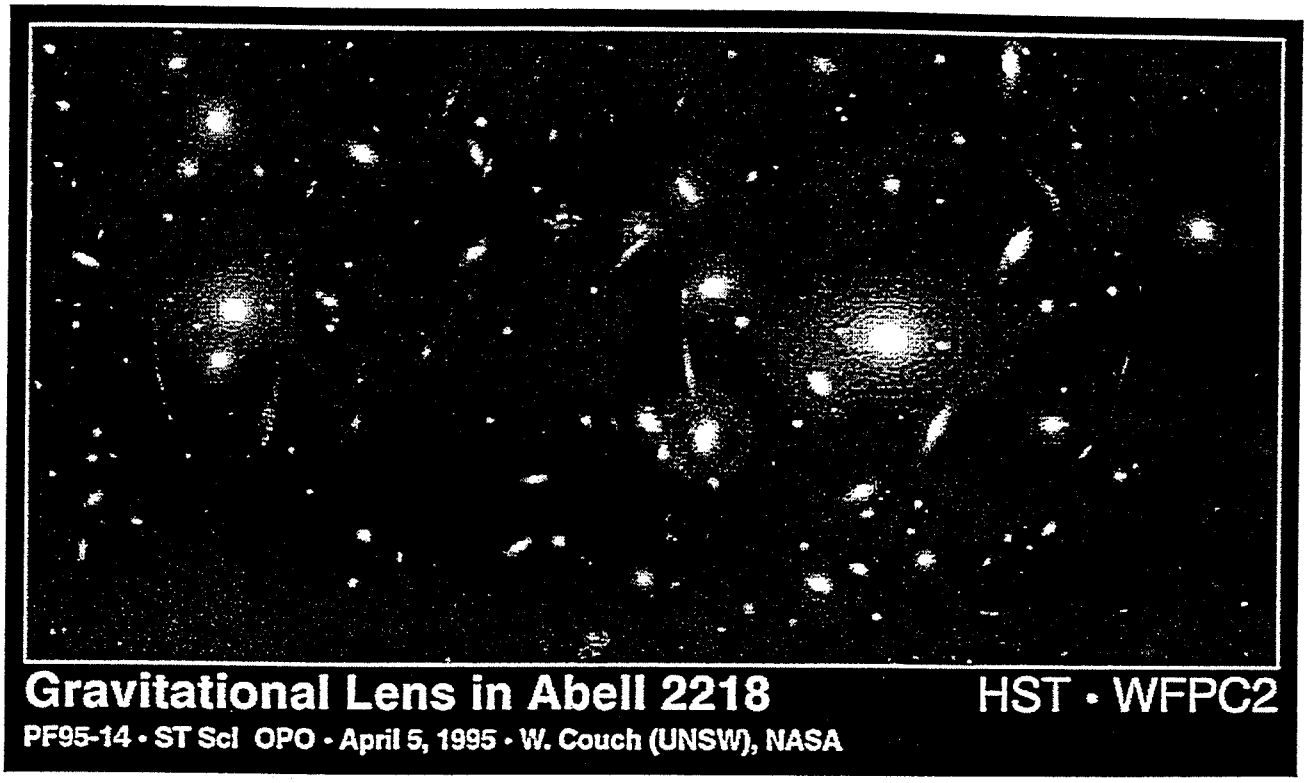

Gravitational Lens in Abell 2218 HST • WFPC2

PF95-14 • ST ScI OPO • April 5, 1995 • W. Couch (UNSW), NASA

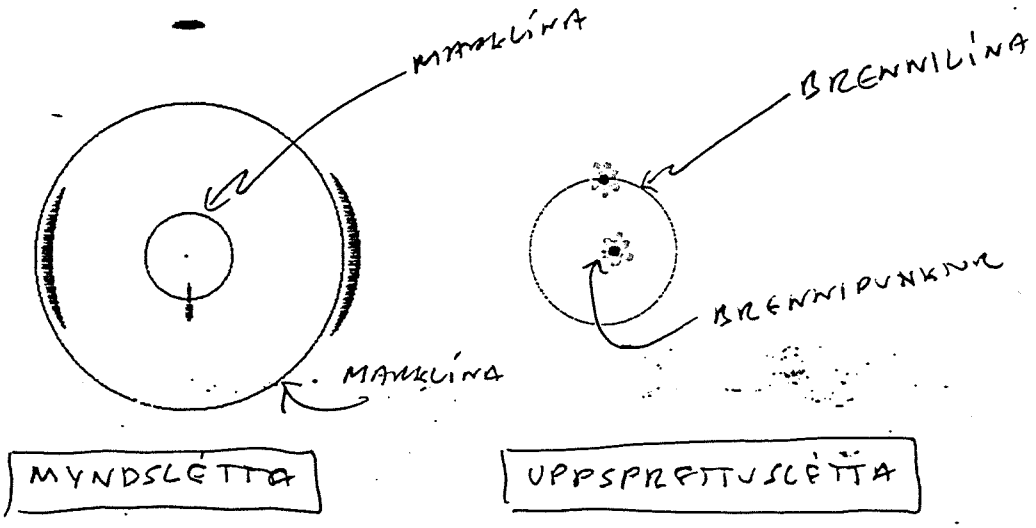

FIG. 18.— Imaging of an extended source by a non-singular circularly-symmetric lens. A source close to the point caustic at the lens center produces two tangentially oriented arc-like images close to the outer critical curve, and a faint image at the lens center. A source on the outer caustic produces a radially elongated image on the inner critical curve, and a tangentially oriented image outside the outer critical curve. Because of these image properties, the outer and inner critical curves are called *tangential* and *radial*, respectively.

NARAYAN & BARTELMANN
1995

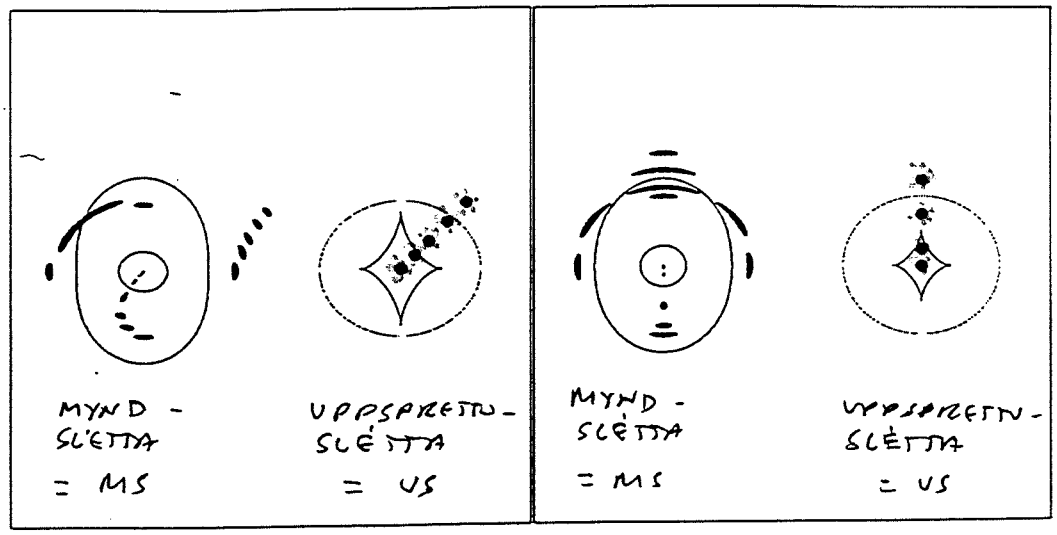

FIG. 19.— Compact source moving away from the center of an elliptical lens. Left panel: source crossing a fold caustic; right panel: source crossing a cusp caustic. In each panel, the diagram on the left shows critical lines and image positions and the diagram on the right shows caustics and source positions.

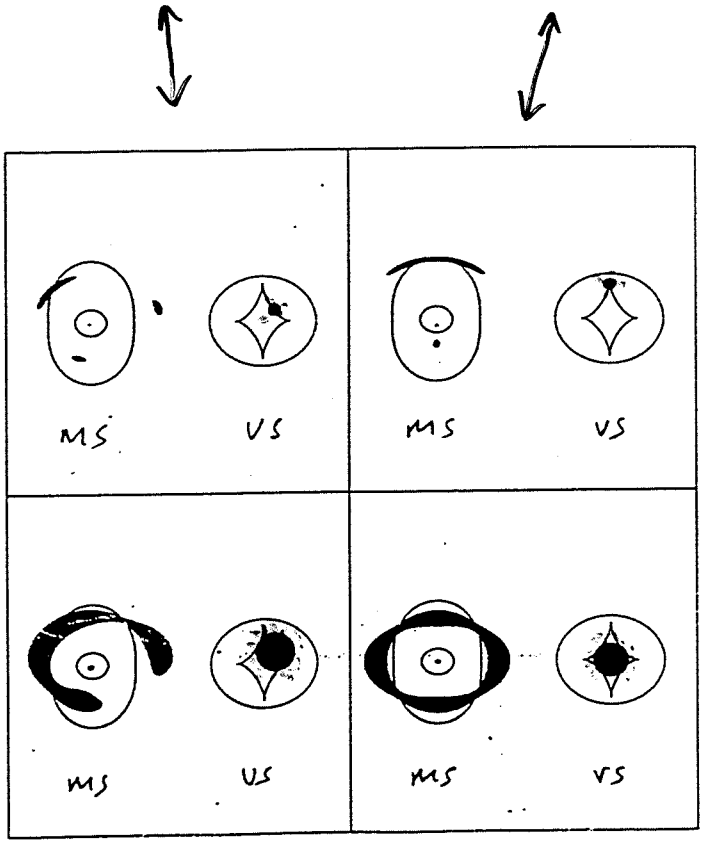

FIG. 20.— Images of resolved sources produced by an elliptical lens. Top panels: Large arcs consisting of two or three merging images are formed when the source lies on top of a fold section (top left panel) or a cusp point (top right panel) of the tangential caustic. Bottom panels: A source which covers most of the diamond-shaped caustic produces a ring-like image consisting of four merging images.

NAKAMAN & BARTELMANN
1995

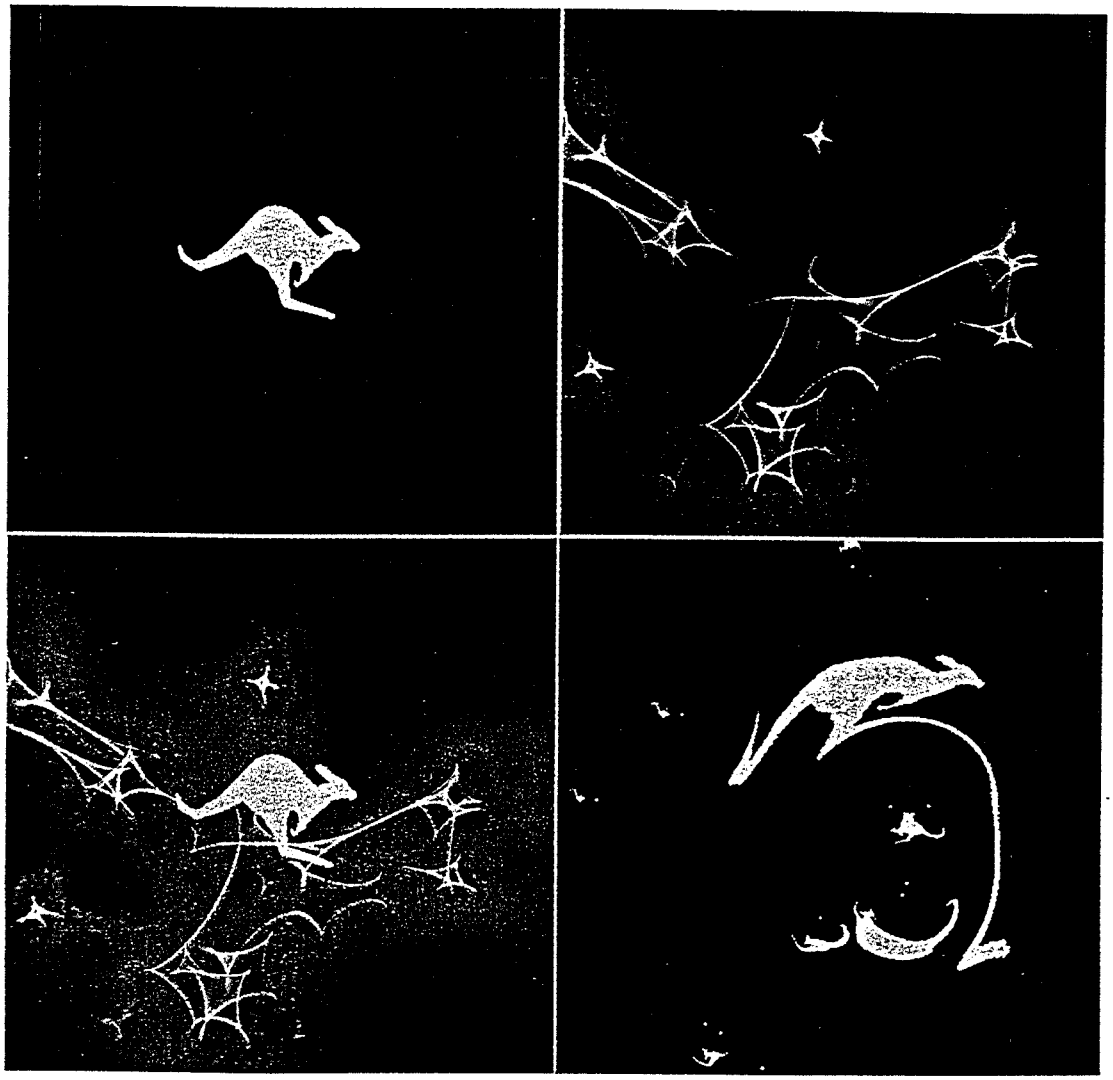

Figure 1 A kangaroo (a) illustrates strong and weak gravitational lensing. About a dozen simulated gravitational lenses produce 'caustic' structures (b), which define regions in the source plane that give rise to multiple images. The yellow lines indicate source positions that correspond to very high magnification, with other colours (red, green, blue) representing increasingly lower magnification. c, The position of the source relative to the caustics. d, The source as seen through the point lenses (marked by red dots). The magnified main image includes a strong giant arc, and there are three other strongly distorted images of the source, and a few fainter mirror-images. Note that the body of the kangaroo is enlarged and distorted, whereas the heel (inside the caustic region) is deformed into a triple arc.

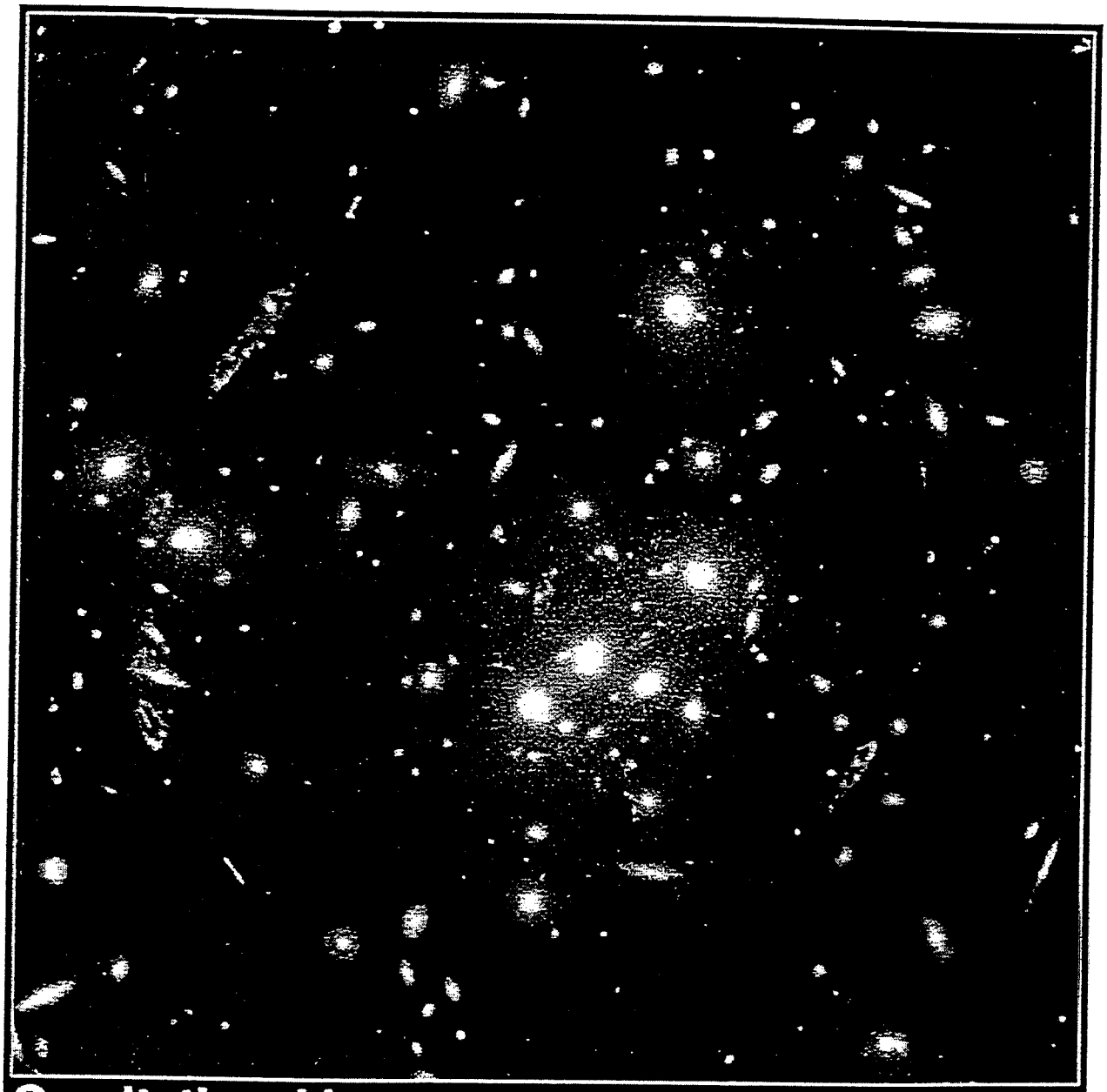

Gravitational Lens Galaxy Cluster 0024+1654

HST • WFPC2

PRC96-10 • ST ScI OPO • April 24, 1996

W.N. Colley (Princeton University), E. Turner (Princeton University),
J.A. Tyson (AT&T Bell Labs) and NASA

PLATE L16

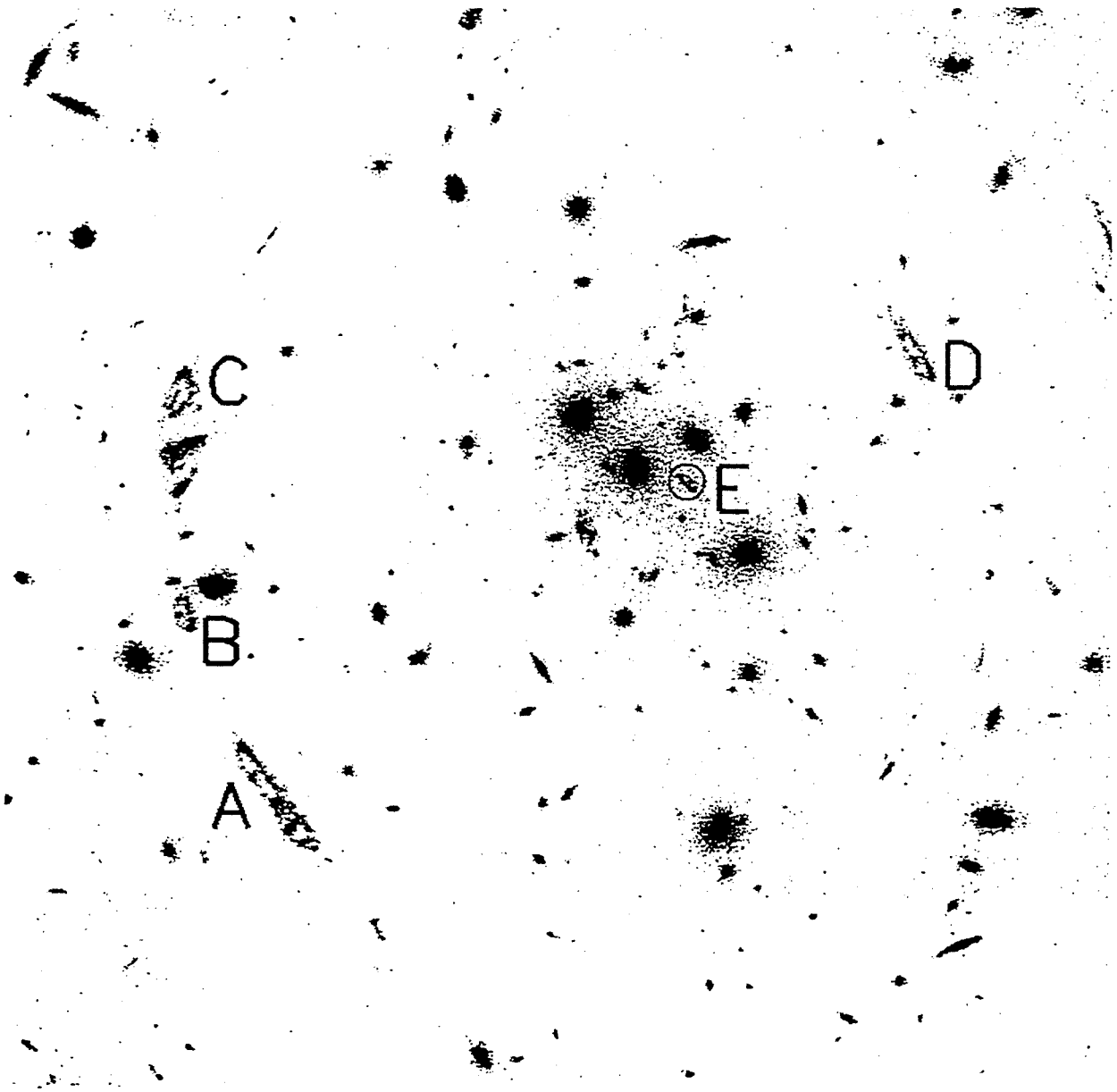

FIG. 2.—Nomenclature for arcs A, B, C, D, and E marked on a stretched monochrome subfield extracted from the blue WFC2 image. The existence of image E constrains the soft core of the main potential.

KASSIOLA, KOVNER & FORT

4. A NUMERICAL MODEL OF THE ARC IN Cl 0024+1654

After the simple one-dimensional analysis of the previous two sections, we now turn to numerical modeling, to see how the qualitative methods compare with more detailed numerics. The numerical analysis was based on an image (Fig. 8) obtained by Koo (1987), who was the first to discover this arc and to bring it to our attention. The redshift of the cluster is 0.39 (Dressler et al.). The redshift of the arc cannot be determined accurately from the present spectroscopic data (Mellier et al. 1991), but is considered to be between 1 and 2.

4.1. *Method of Search*

We used a numerical code (Kovner 1989; Kassiola et al. 1991) that maps points in the image plane into their sources in the source plane.

We considered a three-component lens potential. The first component is a squeezed pseudoisothermal sphere, with potential

$$\Phi = \Theta[b^2 + (1-\epsilon)x^2 + (1+\epsilon)y^2]^{1/2}\,, \tag{25}$$

where b is the core radius, ϵ the ellipticity, and

$$\Theta = 4\pi \frac{\sigma^2}{c^2}\frac{d_{ls}}{d_{os}} \tag{26}$$

is the typical deflection of the potential. The quantities d_{ls} and d_{os} are the angular diameter distances from the lens to the source and from the observer to the source, respectively, and σ is the velocity dispersion of the underlying mass distribution. The squeezed pseudoisothermal sphere represents the traceable mass of the cluster: its visible mass, as well as any unseen mass traced by it. The two other components of the lens potential are two singular isothermal spheres, representing the perturbing clump. These two components are centered on the galaxies G186 and m_1 (see Fig. 8) on either side of the middle segment of the arc. The center of the cluster potential was one of the parameters sought in the model. These parameters were first chosen randomly, within a fixed range of possible values, and then optimized by a gradient method so that the source points satisfy a preimposed condition.

The position of the arc (see Fig. 8) was marked by the end points of its three segments (we took into account the constraints imposed by the length of the arc only, and not by its width). Assuming a source galaxy of elliptical shape, with major axis S_1S_2, three out of these six points should be mapped very close to S_1, and the other three very close to S_2. This can be seen from Figures 1 and 2. It also follows from geometrical considerations described in detail by Blandford & Kovner (1988). Thus we require, as condition for optimization of a model, that the end points are mapped in the source plane as follows: the distances between the source points of each triplet are much smaller than their distances from the sources of the other triplet. More details about the optimization are given in Appendix A. After optimization the source galaxy is reconstructed as an ellipse, with one axis connecting the two triplets, while the size of the other axis can be fixed so as to give to the image the desired thickness. Note that the combination of points in the triplets is different for a right-handed cusp than for a left-handed one (see Appendix A for details).

We took into account the effect of atmospheric smearing by employing the following "smearing" technique: normally the arc consists of a set of "true" points, mapped by the lens to the source(s). To smear, we take around each true point of the arc $6n$ other points at the vertices of n hexagons of gradually increasing dimension. The dimension and the number n of hexagons are chosen so as to give a width of $\sim 1''$ to the arc (the observed width, roughly equal to the seeing of the observations).

4.2. *The Model*

We show one of our best models in Figure 9. The arc is formed by a single source galaxy near a perturbed right-handed cusp. Each of its segments is singly imaged. The cusp is naked and thus does not create any other images. In agreement with our qualitative analysis in § 3.2, we could not find any successful model of the arc with a perturbed left-handed cusp. This is apparently related to the length of the middle image: recall that when a left-handed cusp is perturbed, the length of the middle image, in general very small, is essentially determined by the slope of the perturbation, which depends on the

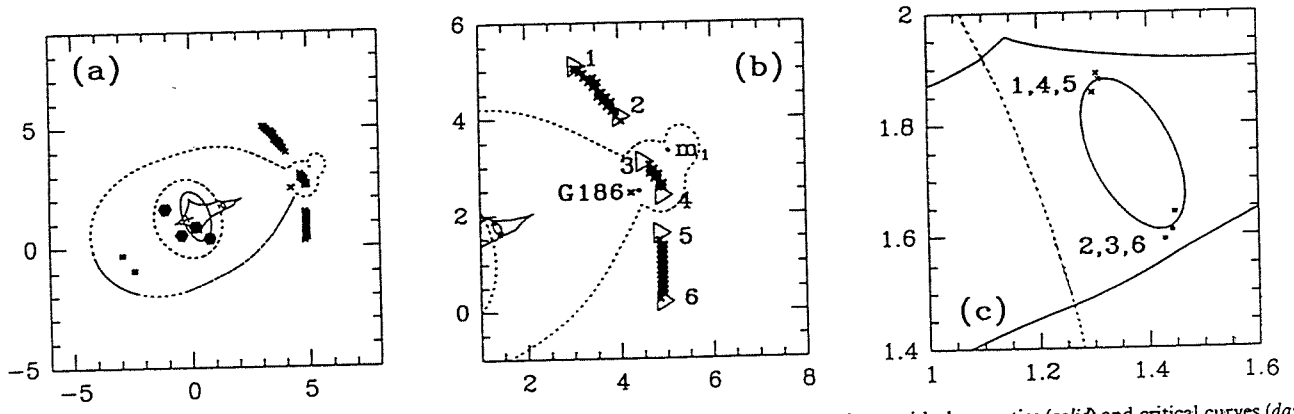

FIG. 9.—A numerical model of the triple arc, based on earlier observations. (*a*) The source and image planes with the caustics (*solid*) and critical curves (*dashed*). The center of the main potential (cluster) is noted by a cross, while the centers of the two perturbing clumps are small dots. A small extra image (*cross*) can be seen near the center of one of the clumps. The positions of the five brightest galaxies of the cluster are shown by black hexagons (for illustration only; they were not taken explicitly into account in the lens potential). The source galaxy can also be seen, near the tip of the perturbed cusp. The positions of the edges of the fourth arclet are marked by black squares. (*b*) A closer view of the image plane near the arc. The centers of the triangles numbered 1, 2, ..., 6 are the markers used in the numerical search. The positions of the two perturbing clumps centered on the galaxies 186 and m_1 are also shown (centers marked by small filled circles). There is a small extra image (*cross*) near the center of G186, which should be covered by the galaxy and thus not detected. (*c*) A closer view of the source galaxy. The points numbered 1, 2, ..., 6 are the sources of the markers shown in (*b*). The scale of the figure is 1 unit = 7".2.

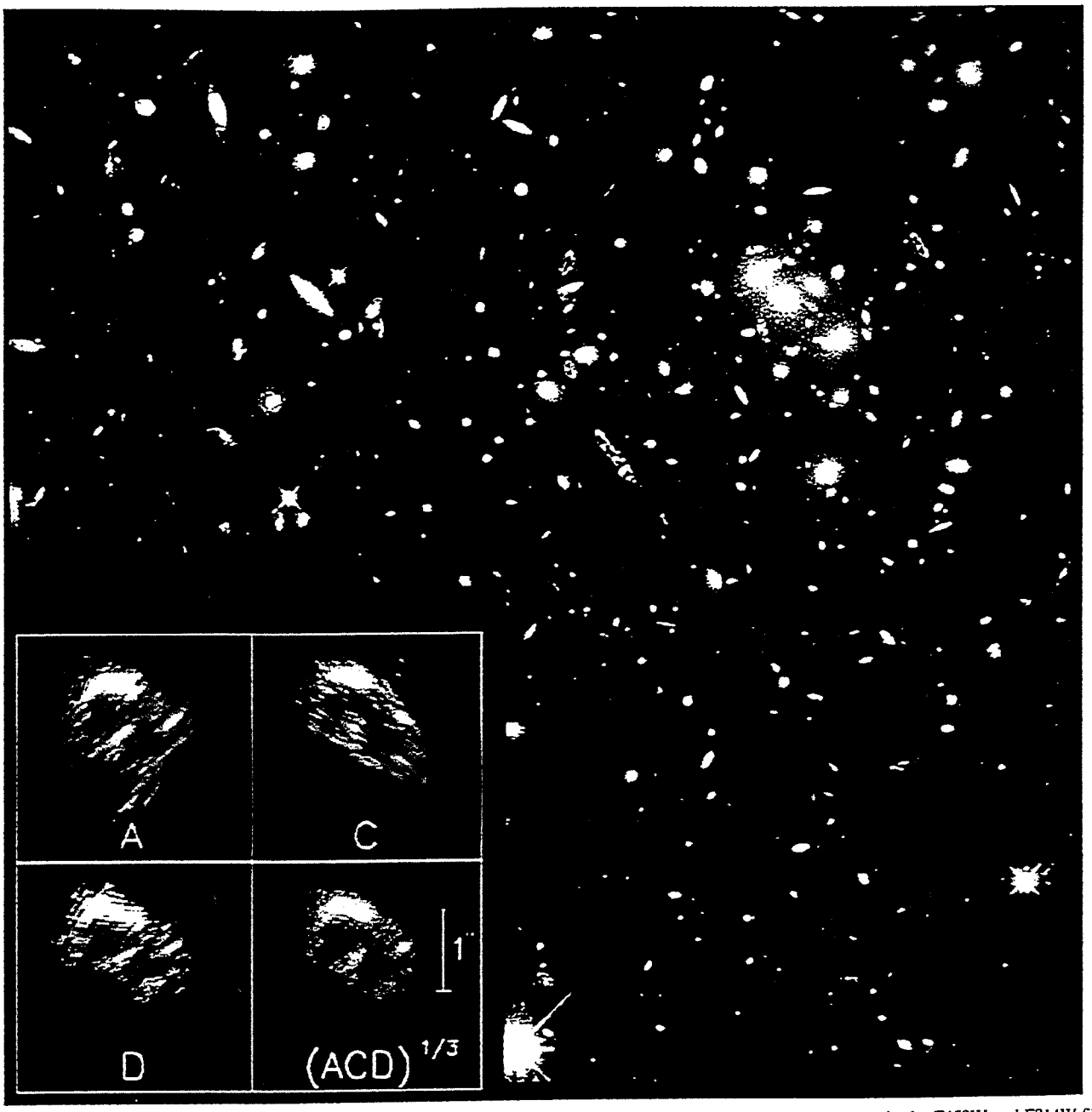

FIG. 1.—Color image of the field of the massive $z = 0.39$ cluster 0024+1654 generated from co-added 15,000 s imaging data in the F450W and F814W filters on the *HST* WFC2 chips. North is up and east is left. The longest side of the image is 2.'7. Five blue arcs, each an image of the same background source at much higher redshift, may be seen. Three of them, two arcs to the southeast and one counterarc to the northwest, are highly magnified. Our reconstruction of the source (see text) by unlensing each of these longest arcs is shown in the inset. The source-plane scale is indicated by a 1" bar. Note that the resolution is greater along the long axis of the arcs.

COLLEY, TYSON, & TURNER (see 461, L84)

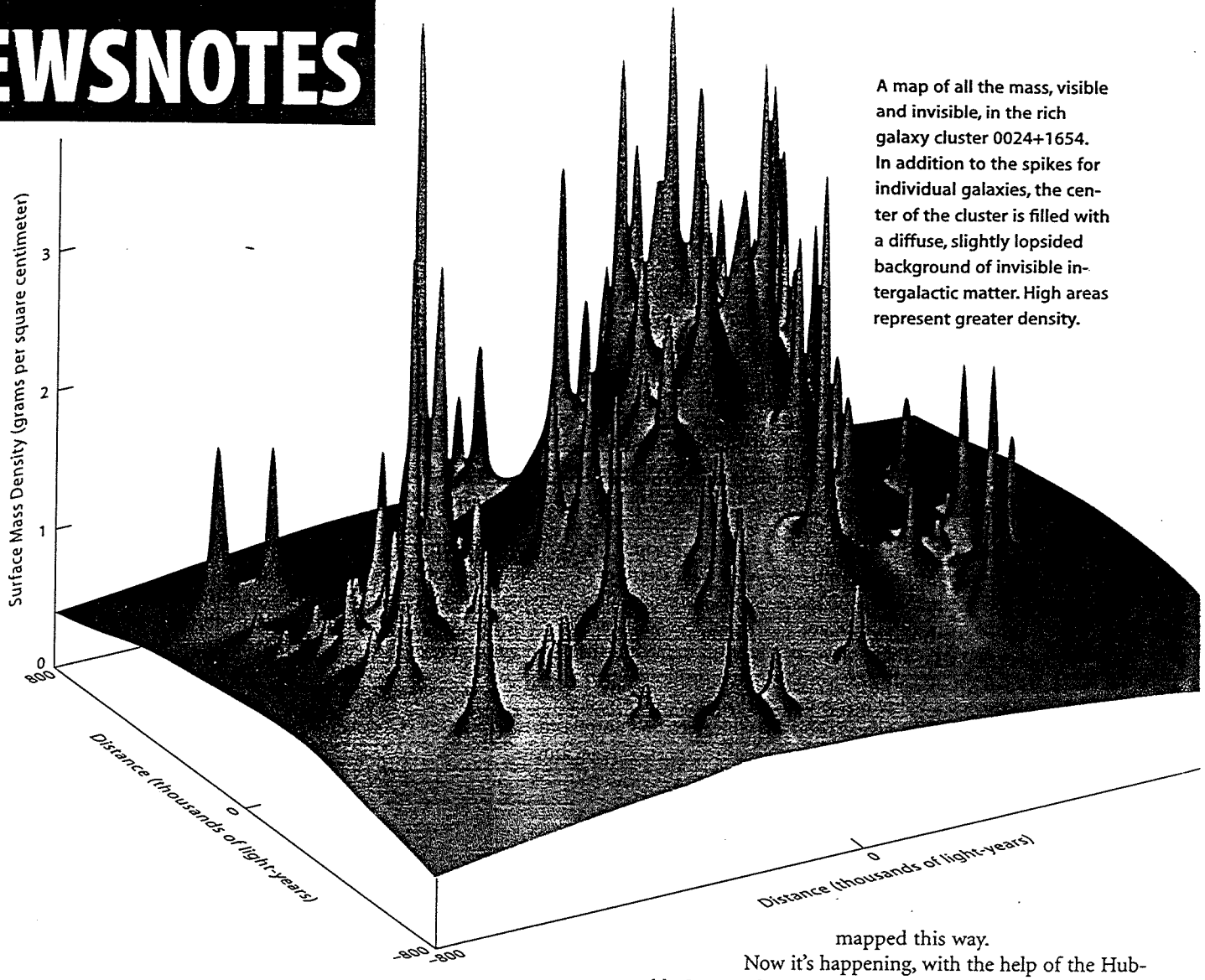

A map of all the mass, visible and invisible, in the rich galaxy cluster 0024+1654. In addition to the spikes for individual galaxies, the center of the cluster is filled with a diffuse, slightly lopsided background of invisible intergalactic matter. High areas represent greater density.

Dark Matter on Display

THE UNIVERSE CONTAINS between 20 and 200 times more mass than all the stars and galaxies we see. This invisible stuff is well hidden, but it reveals itself in one sure way: by its gravity.

When the first gravitational lenses were discovered in 1979, astronomers had high hopes of measuring the total mass of everything in a galaxy, both visible and invisible, by the galaxy's lensing effect on light from objects behind it. Perhaps, they thought, even larger concentrations of dark matter could eventually be mapped this way.

Now it's happening, with the help of the Hubble Space Telescope. Hubble images of galaxy clusters, such as CL 0024+1654 on the cover of the January *Sky & Telescope*, show dramatic lensing distortions of faint blue galaxies in the distant background. Recently three researchers at Bell Laboratories/Lucent Technologies worked out an accurate map of the mass that causes the lensing in this particular cluster.

Greg Kochanski, Ian Dell'Antonio, and J. Anthony Tyson tested more than a million models of mass distribution in the cluster. They narrowed in on the one that best reproduced the gravitational bumps and wiggles distorting the background images. Their density map (above) includes strong peaks for the individual cluster galaxies. In some cases, the researchers were able to determine the most precise masses measured for any galaxy to date.

No large galaxy-size mass concentrations were found that did not correspond to a visible object. However, many of the galaxies turned out to be surrounded by wide halos of dark matter, which show up on the map as bulges around the bottoms of the spikes. Other galaxies lacked big halos.

Most of the cluster's mass, however, proved to be in a large, diffuse, somewhat

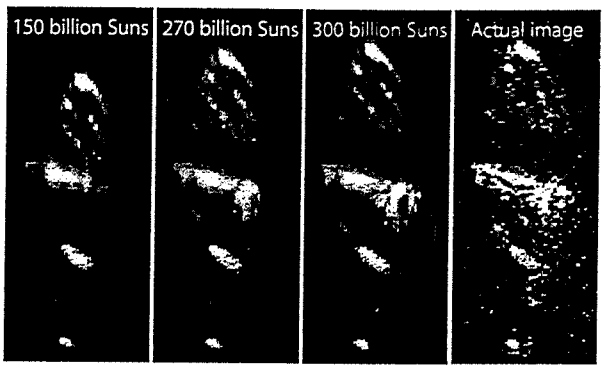

Weighing a gravitational lens. Kochanski, Dell'Antonio, and Tyson computed the distorting effects of the central red galaxy upon light from a far more distant, blue one. By raising the red galaxy's mass from 150 to 300 billion Suns *(first three panels)*, the scientists were able to account for the Hubble Space Telescope view of both objects *(right)*.

ILLUSTRATIONS COURTESY G. KOCHANSKI, I. DELL'ANTONIO, AND J. A. TYSON

VEIK LINSUHRIF

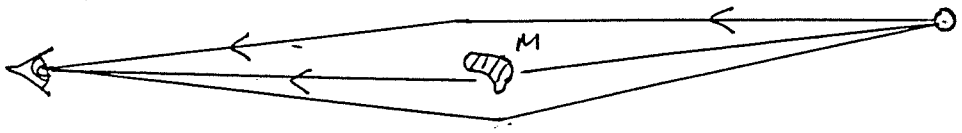

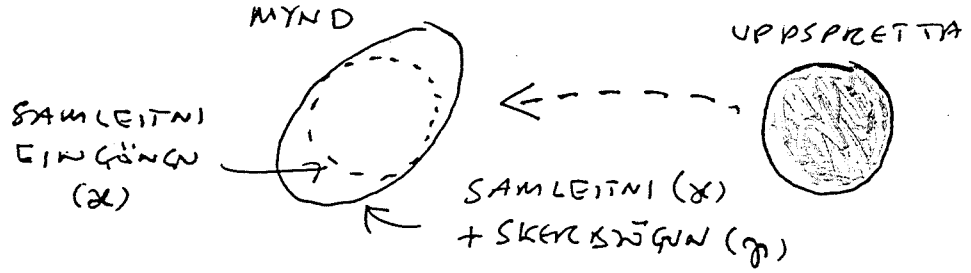

JAKOBÍFYLKIÐ MÁ SKRIFA SEM :

$$J = \begin{pmatrix} 1-\kappa-\gamma_1 & -\gamma_2 \\ -\gamma_2 & 1-\kappa+\gamma_1 \end{pmatrix}$$

$$= (1-\kappa)\begin{pmatrix} 1 & 0 \\ 0 & 1 \end{pmatrix} - \gamma \begin{pmatrix} \cos 2\phi & \sin 2\phi \\ \sin 2\phi & -\cos 2\phi \end{pmatrix}$$

↑ SAMLEITNI — ↑ SKERSBÖGUN — STEFNA BÖGUNAR

ÞAR SEM : $\kappa = \frac{1}{2}\Delta\psi = \frac{1}{2}\left(\frac{\partial^2\psi}{\partial\theta_{I1}^2} + \frac{\partial^2\psi}{\partial\theta_{I2}^2}\right)$

$$\gamma = \left(\gamma_1^2 + \gamma^2\right)^{1/2}$$

$$\gamma_1 = \frac{1}{2}\left(\frac{\partial^2\psi}{\partial\theta_{I1}^2} - \frac{\partial^2\psi}{\partial\theta_{I2}^2}\right)$$

$$\gamma_2 = \frac{\partial^2\psi}{\partial\theta_{I1}\partial\theta_{I2}} = \frac{\partial^2\psi}{\partial\theta_{I2}\partial\theta_{I1}}$$

STÆKKUN/MÖGNUN : $\mu = \frac{1}{\det J} = \frac{1}{(1-\kappa)^2 - \gamma^2}$

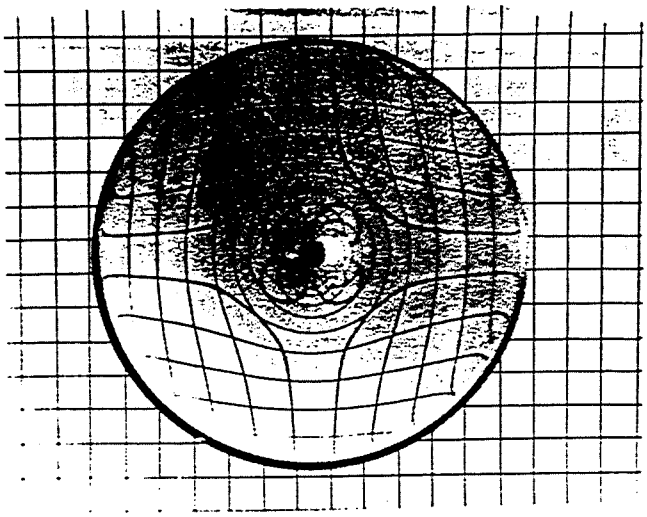

(a)

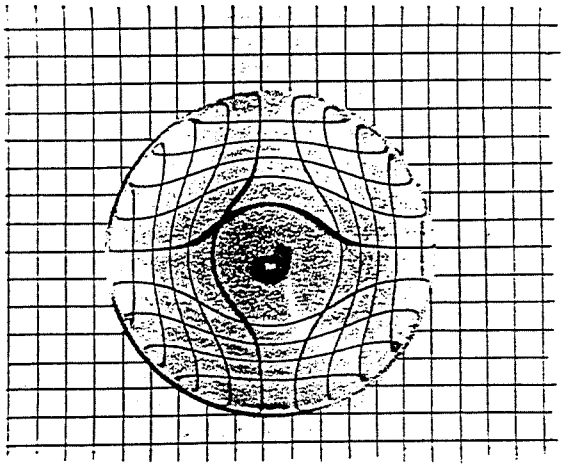

(c)

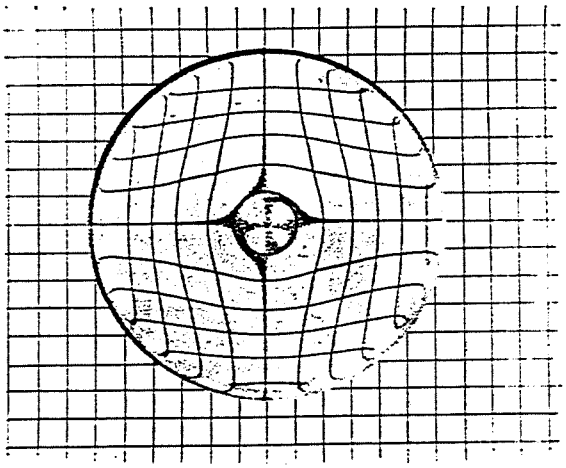

(b)

Fig. 8. Square grid as seen through the lenses: (a) point mass; (b) constant density sphere; (c) isothermal gas sphere.

NANDOR & HELLIWELL
1996

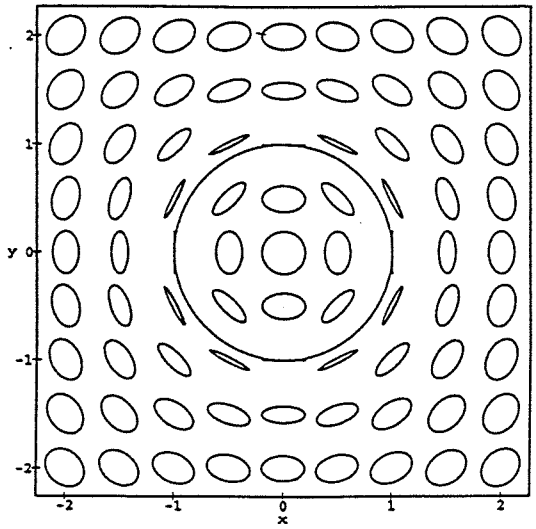

Fig. 2. The ellipse field due to a point mass. Note that the large principal axes are fixed. For convenience we also show the critical curve

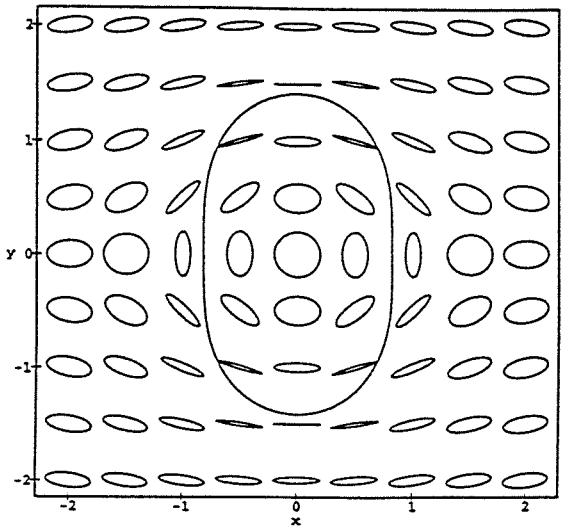

Fig. 4. The ellipse field due to a point mass and an additional shear. The critical curve is also shown

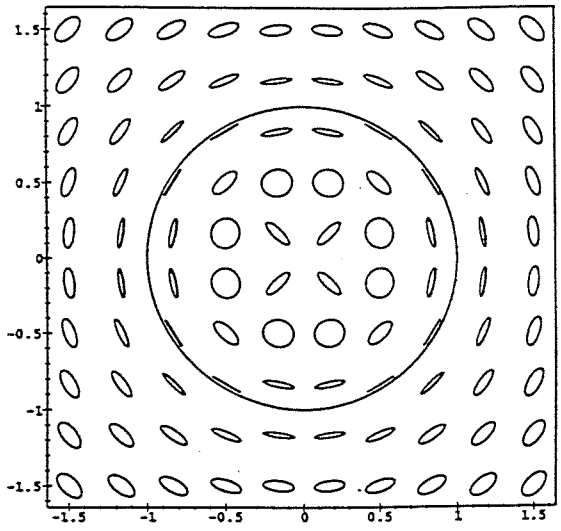

Fig. 5. Ellipse field of the lens as given by an isothermal sphere with $\kappa_0 = 0.5$. Note the tangential and radial stretching of the ellipses near the critical line and the center

SCHNEIDER & KAYSER
A&A 295, 1 '95

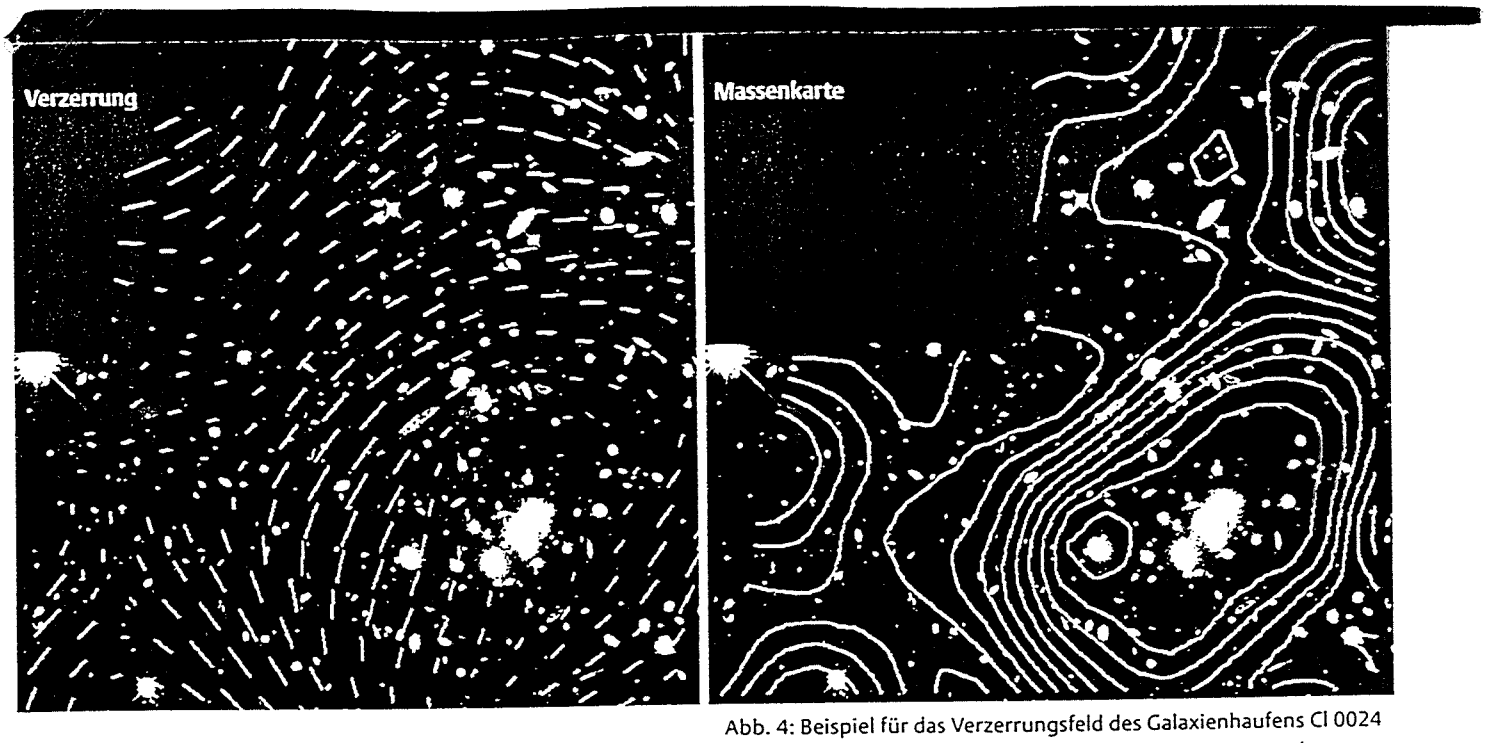

Abb. 4: Beispiel für das Verzerrungsfeld des Galaxienhaufens Cl 0024 (links) und die Massenkarte, die aus diesen Verzerrungen rekonstruiert wurde (rechts). Der Galaxienhaufen wurde mit dem Hubble Space Telescope aufgenommen, das Verzerrungsfeld wurde mit dem Canada-France-Hawaii-Teleskop gemessen. Oberhalb des Haufenzentrums ist ein dreigeteilter Bogen zu sehen. Die Kantenlänge des Bildes beträgt etwa 1.5 Bogenminuten. (Die Bilder wurden freundlicherweise von C. Seitz zur Verfügung gestellt.)

abgeleitet wurden, stellte sich heraus, daß sie nicht statisch sein können, d.h. sie müssen sich entweder ausdehnen oder zusammenziehen. Zu dieser Zeit war die allgemeine Ausdehnung des Universums noch nicht bekannt. Einstein führte daraufhin einen weiteren Ausdruck in die Gleichungen der Allgemeinen Relativitätstheorie ein, der solche statischen Modelle ermöglicht. Er wird durch die sogenannte kosmologische Konstante gekennzeichnet. Als bekannt wurde, daß sich das Universum tatsächlich ausdehnt, waren keine statischen Weltmodelle mehr nötig und damit auch keine kosmologische Konstante. Einstein bezeichnete daraufhin seine Einführung der kosmologischen Konstante als die »größte Eselei seines Lebens«. Trotzdem gab es sie nun, und sie erfährt seit dieser Zeit immer wieder neues Interesse, weil es Beobachtungen gibt, die besser mit solchen kosmologischen Modellen übereinstimmen, die die kosmologische Konstante enthalten. Die Hubble-Konstante schließlich mißt, wie schnell sich das Universum heute ausdehnt.

Diese drei Parameter sind nicht gut bekannt. Wir wissen nur, daß der Dichteparameter größer als etwa 0.2 sein muß und nicht wesentlich größer als eins sein kann. Es gibt verschiedene Argumente, daß die kosmologische Konstante kleiner sein sollte als etwa 0.6 bis 0.7. Außerdem gibt es die theoretische Vorliebe der sogenannten Inflationären Kosmologie, daß die Summe aus dem Dichteparameter und der kosmologischen Konstanten gleich eins sein sollte. Die Unsicherheit ist groß, und jedes Argument ist willkommen, das diese Unsicherheit durch Beobachtungen zu vermindern hilft. Die Hubble-Konstante ist vergleichsweise gut bekannt. Die Ungenauigkeit jüngster Messungen ist auf nur noch etwa 20 Prozent gesunken.

Entstehung von Strukturen

Außer einer Beschreibung, wie das Universum als Ganzes beschaffen ist, enthalten die kosmologischen Modelle eine Theorie, wie sich Strukturen im Weltall entwickelt haben. Diese Theorie sagt aus, daß in einer sehr frühen Phase des Universums sehr kleine Dichteschwankungen angelegt wurden, die dann durch ihre Schwerkraft Materie aus der Umgebung anziehen und dadurch wachsen konnten. Wir kennen den Ursprung dieser Dichteschwankungen nicht. Dennoch scheint die Vorstellung ihres Wachstums aufgrund der Gravitationsinstabilität richtig zu sein. Um eine Vorstellung von der Entstehung der Strukturen im Weltall zu gewinnen, ist es wichtig zu wissen, welche Eigenschaften die Dichteschwankungen hatten. Zu diesem Zweck kennzeichnet man sie durch ihre Größe und durch ihre Höhe. Der Zusammenhang zwischen der mittleren Höhe der Schwankungen und ihrer Größe wird als Störungsspektrum bezeichnet. Die Form dieses Störungsspektrums hängt davon ab, woraus sich die Materie zusammensetzt, die das Universum dominiert. Die Amplitude des Spektrums ist davon unabhängig und muß aus Beobachtungen bestimmt werden. Form und Amplitude des Störungsspektrums sind wesentlich für den Verlauf und das Ergebnis der Strukturentwicklung im Universum.

Im Lauf der Zeit wachsen die Dichteschwankungen immer weiter an, weil sie Materie aus ihrer Umgebung anziehen. Das Wachstum hängt aber davon ab, welche Werte die kosmologischen Parameter haben, insbesondere der Dichteparameter. Das liegt daran, daß das Universum sich umso schneller ausdehnt, je weniger Materie seine Ausdehnung bremst, je kleiner also der Dichteparameter ist. In einem Universum mit geringer Dichte wird die Ausdehnung immer schneller, je älter es wird. Die Ausdehnung läßt die Teilchen des kosmischen Materials voneinander wegfliegen. Um weiter anwachsen zu können, muß eine Dichtefluktuation zunächst diese Fluchtbewegung durch ihre Schwerkraft überwinden. Das wird umso schwieriger, je schneller die Fluchtbewegung wird. Eine Folge davon ist, daß in einem Universum mit geringer Materiedichte, also kleinem Dichteparameter, das Wachstum der Strukturen im Lauf der kosmischen Entwicklung zum Stillstand kommt. Das wiederum bedeutet, daß alle Strukturen, die wir heute sehen, also z.B. die Galaxienhaufen, umso früher entstanden sein müssen, je kleiner der Dichteparameter ist, weil sie in diesem Fall von einem bestimmten Zeitpunkt an einfach nicht mehr weiter wachsen konnten.

Entwicklung von Galaxienhaufen

Indem wir Galaxienhaufen bei immer größeren Entfernungen beobachten, sehen wir sie auch in immer früheren Stadien ihrer Entwicklung, weil das Licht von

VEIK LINSUHRIF OG TALNING VETRARBRAUTA

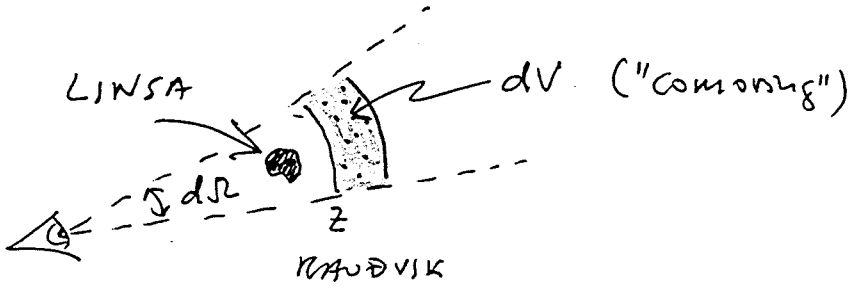

FJÖLDI VETRARBRAUTA Í dV MEÐ LJÓSAFL MILLI L OG L+dL: $dN = \phi(L,z)\,dL\,dV(z)$

↑ LÝSIFALL (LUMINOSITY FUNCTION)

FJÖLDI VETRARBRAUTA MEÐ RAUÐVIK MILLI z OG z+dz Í dΩ:

$$N(z)\,dz = \underbrace{\left\{\int_{L_{min}}^{\infty} \phi(L,z)\,dL\right\}}_{=\Phi(L_{min},z)} dV(z)$$

LINSUHRIF VALDA ÞVÍ AÐ ATHUGANDI MÆLIR:

BIRTU: $f' = \mu \frac{L}{4\pi d_L^2}$ (MÖGNUN)

STEFNU: $d\Omega' = \mu\, d\Omega$ (STÆKKUN)

$$\Rightarrow \quad dN' = \phi\left(\frac{L}{\mu},z\right) dL \frac{dV(z)}{\mu}$$

OG

$$N'(z)\,dz = \underbrace{\left\{\int_{L_{min}/\mu}^{\infty} \phi\left(\frac{L}{\mu},z\right) dL\right\}}_{\bar{\Phi}\left(\frac{L_{min}}{\mu},z\right)} \frac{dV(z)}{\mu}$$

SÆMILEGA GÓÐ MÆLGUN (FYRIR BIL Í L): $\Phi(L,z)$ OG $[L(z)]^{-\beta}$

ATH: $\beta \equiv -\frac{d\log\Phi(L,z)}{d\log L} = \beta(L,z)$

Í MÆLINGUM ER STUNDUM NOTAÐ Í STAÐ $f = \frac{L}{4\pi d_L^2}$ OG ÞÁ ER OFTAST UNNIÐ MEÐ STÆRÐINA

$$\gamma \equiv \frac{d\log\Phi(m,z)}{dm} = \frac{\beta}{2.5}$$

$$\Rightarrow \quad N'(z) = \mu^{\beta-1} N(z) = \mu^{2.5\gamma-1} N(z)$$

$$\Rightarrow \quad \mathbb{N}' = \int_0^\infty N'(z)\,dz \approx \mu^{\beta-1}\int_0^\infty N(z)\,dz = \mu^{\beta-1}\,\mathbb{N}$$

β	γ	LINSUHRIF
<1	$<0{,}4$	STÆKKUN $\longrightarrow$ FÆRRI VETRARBR.
1	$0{,}4$	LINSUHRIF: ENGIN Á N
>1	$>0{,}4$	MÖGNUN $\longrightarrow$ FLEIRI VETRARBR.

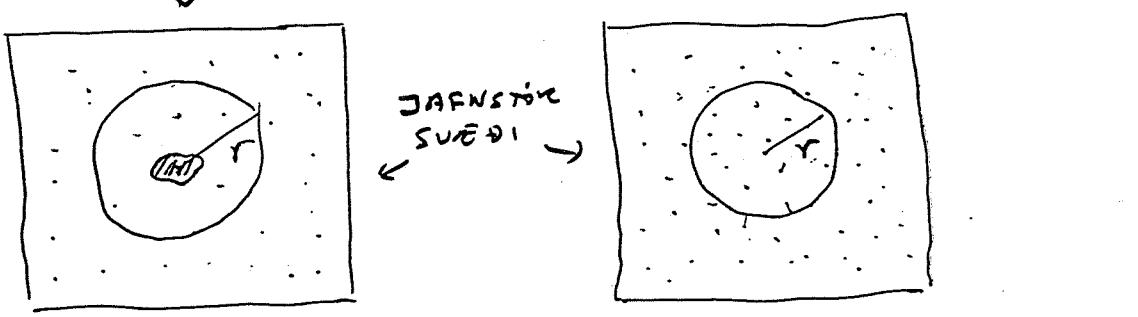

SVÆÐI UMHVERFIS LINSU: $N'(z)$ OG $\mathbb{N}'$

SVÆÐI AN LINSU: $N(z)$, $\beta=\beta(z)$ OG $\mathbb{N}$

$$\Rightarrow \quad \mu = \mu(r)$$

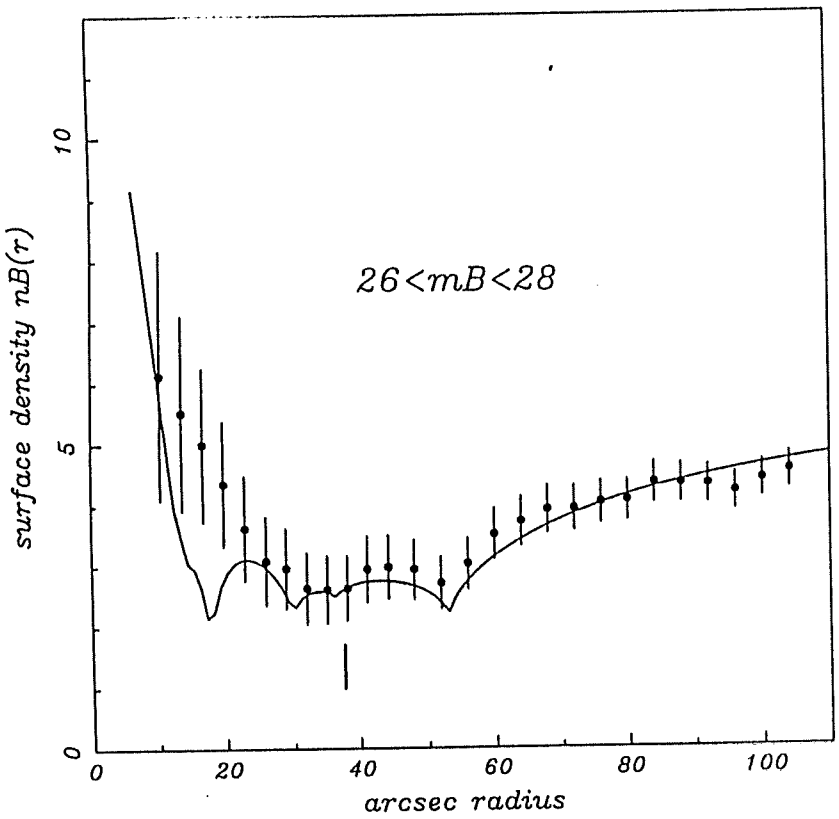

Fig. 2. Depletion curve obtained in Cl0024+1654 from galaxy counts in the range $26 < B < 28$ for the B-selelected galaxies. The data are the filled circles with error bars. We see that a depletion is detected, with a minimum starting at $R_B = 30$ arcsec. The full line show a fit with the model and core radius obtained by KKF.

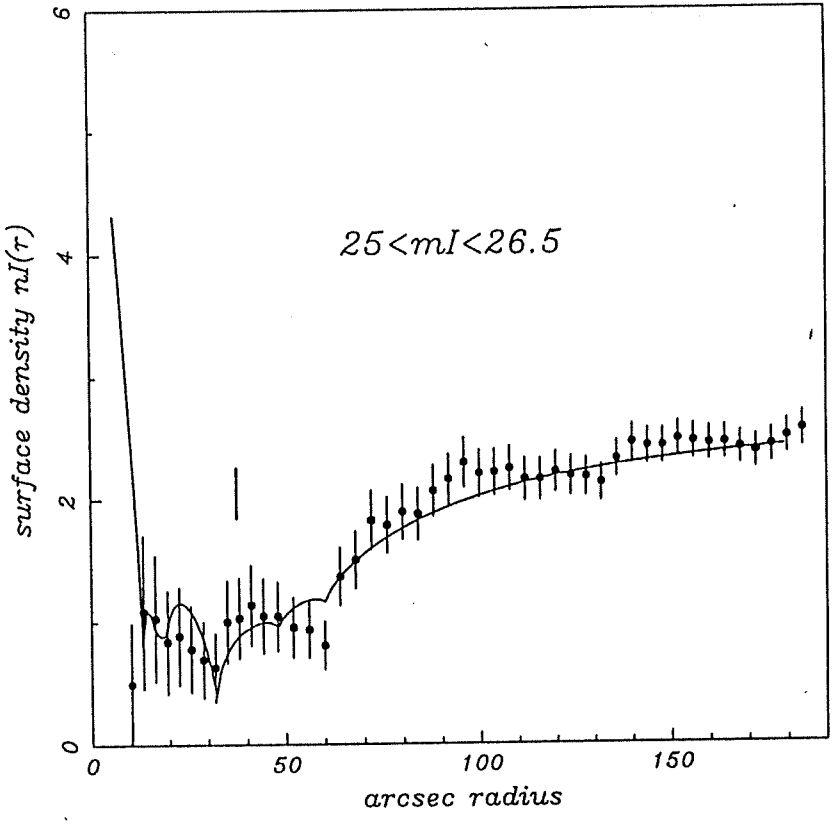

Fig. 3. Same plot as figure 2 for the I sample. The width of the depletion spread on a larger area. The minimum radius is almost similar to the B galaxies. The *last critical radius* is defined as the position where the depletion curve starts to increase. This corresponds to $R_I = 60$" arcsec.

FORT, MELLIER & DANTEL-FORT
1997

SEINKUN OG H_0

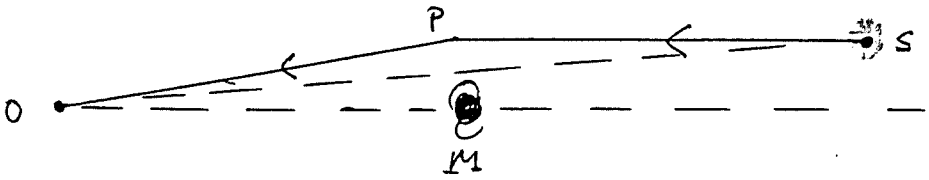

ÁN M FÆRI LÓSMERKI BEINA BRAUT FRÁ S TIL O. TILVIST M SEINKAR MERKINU UM TÍMA δt:

$$\delta t = \delta t_{SHAPIRO} + \delta t_{BRAUT}$$

↑ ÁHRIF ÞYNGDAR LINSU Á FERÐATÍMANS

↑ VEGALENGDIN SPO ER LENGRI EN SO.

$$\delta t_{SHAPIRO} = (1+z_d)\frac{2}{c^3}\left|\int \Phi\, ds\right| = -\frac{(1+z_d)\,D_{od}\,D_{os}}{c\,D_{ds}}\,\psi$$

↑ ÁHRIF ÚTÞENSLU ALHEIMS

↑ NEWTÓNSKT ÞYNGDARMÓÐTTI

↑ ALM. NEIKVÆÐ STÆRÐ

$$\delta t_{BRAUT} = (1+z_d)\,\frac{D_{os}\,D_{od}}{2c\,D_{ds}}\,(\theta_I^2 - \theta_S^2)$$

TVÆR MYNDIR A OG B:

TÍMAMUNUR Á BLOSSA Í A OG BLOSSA Í B:

$$\Delta t = |\delta t_A - \delta t_B| = \frac{(1+z_d)\,D_{os}\,D_{od}}{c\,D_{ds}}\left\{\frac{1}{2}\left[(\theta_A-\theta_S)^2 - (\theta_B-\theta_S)^2\right] - \left[\psi(\theta_A) - \psi(\theta_B)\right]\right\}$$

ALM. ER

$$D = \frac{c}{H_0}\,f(z, \Omega_0, \lambda_0, \varphi_0) \approx \frac{c}{H_0}\,z \quad \text{ef } z \ll 1$$

↑ HEIMSLÍKAN

LÍNULÍKAN: ψ, θ_S

MÆLINGAR: $\Delta t, \theta_A, \theta_B, z_d, z_s$

MJÖG STERK !

↓

STERK LINSUMMF

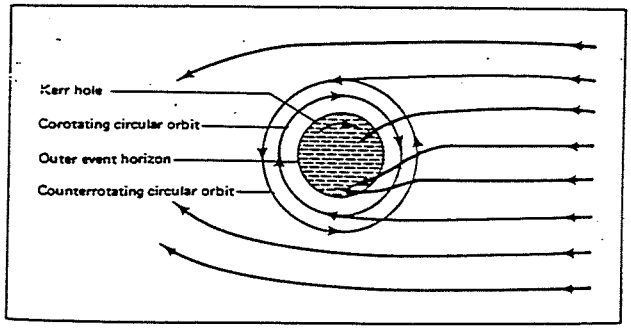

LINSA :

KERR SVARTHOL

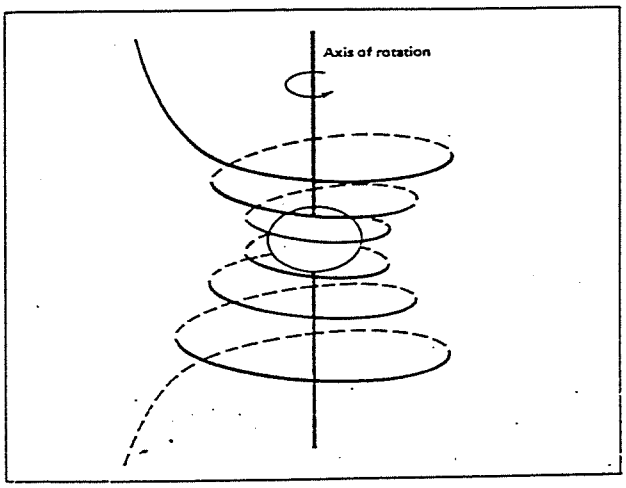

KAUFMANN
1977

SÉRSTÆÐAR LINSUR

LINSA :

ORMAGÖNG

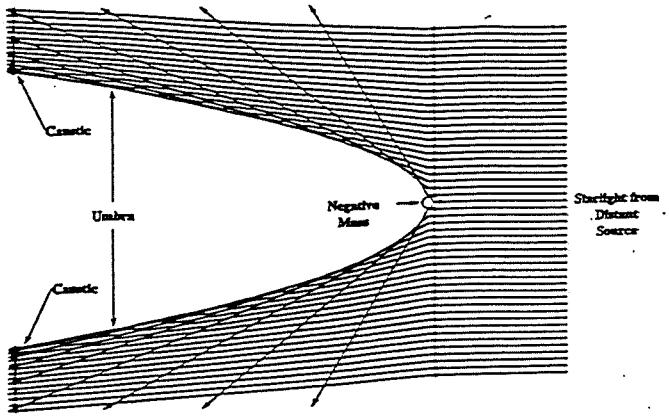

CRAMER ET AL.
PHYS REV D 51,
3117 '95